Shallow V-Shape Nanostructured Pit Arrays in Germanium Using Aqua Regia Electroless Chemical Etching

Ibtihel Chaabane [1,2], Debika Banerjee [1], Oualid Touayar [2] and Sylvain G. Cloutier [1,*

[1] Department of Electrical Engineering, École de Technologie Supérieure, 1100 Notre-Dame Ouest, Montréal, Québec, QC H3C 1K3, Canada; ibtihel.chaabane.1@etsmtl.net (I.C.); debika.banerjee.1@etsmtl.net (D.B.)
[2] Department of Physics and Instrumentation, National Institute of Applied Science and Technologies, Charguia, Tunis 1080, Tunisia; touayar.walid@planet.tn
*** Correspondence: sylvaing.cloutier@etsmtl.ca; Tel.: +1-514-396-8897

Abstract: Due to its high refractive index, reflectance is often a problem when using Germanium for optoelectronic devices integration. In this work, we propose an effective and low-cost nano-texturing method for considerably reducing the reflectance of bulk Germanium. To do so, uniform V-shape pit arrays are produced by wet electroless chemical etching in a 3:1 volume ratio of highly-concentrated hydrochloridric and nitric acids or so-called aqua regia bath using immersion times ranging from 5 to 60 min. The resulting pit morphology, the crystalline structure of the surface and the changes in surface chemistry after nano-patterning are all investigated. Finally, broadband near-infrared reflectance measurements confirm a significant reduction using this simple wet etching protocol, while maintaining a crystalline, dioxide-free, and hydrogen-passivated surface. It is important to mention that reflectance could be further reduced using deeper pits. However, most optoelectronic applications such as photodetectors and solar cells require relatively shallow patterning of the Germanium to allow formation of a pn-junction close to the surface.

Keywords: Germanium; wet electroless etching; aqua regia; nanostructures; optical properties

1. Introduction

The instability of Germanium dioxide (GeO_2) was a primary cause for the abandonment of Germanium (Ge) in favor of Silicon as the premier material platform for microelectronics [1,2]. Nevertheless, Ge still offers many unique properties for optoelectronic devices [3–8], especially for near-infrared applications [9].

However, a major inconvenience with bulk Ge is its high refractive index, which causes large reflections, preventing efficient light coupling. In the last two decades, nanoscale texturing has proved to be a successful approach to reduce the broadband reflectance of semiconductor surfaces [10–14]. While many low-cost nano-texturing processes were pioneered for silicon [15–19], researchers have been searching for an equivalent approach to achieve uniform and low-cost anti-reflection for bulk Germanium. Some earlier reports focused on electrochemical etching [20–24], where electric fields are used to drive the reaction. Different types of etching agents for various concentrations and etching times were used and encouraging results were achieved using this process [20]. To allow for large-scale manufacturing at low costs, it would be better if an electroless approach could achieve similar results.

Since no good electroless recipe was found, we went back to the roots of chemical wet etching for microelectronics. With the push to develop microelectronics, researchers quickly sought low-cost chemical etching processes to achieve uniform cleaning and etching [2,20,22,25–32]. Early works

quickly converged around two main standard cleaning (SC) protocols pioneered in the late 1960s and early 1970s [25,33].

In the last decade, some research groups have attempted to adapt these standard protocols for Germanium. Regarding HCl-based cleaning protocols, the transfer of aqueous-based cleaning (H_2O:H_2O_2:HCl) from Silicon to Germanium was first attempted as early as 1970, but reports concluded that the protocols should be adjusted to correct for the solubility of GeO_2 in water [34]. More recently, reports looking at the effectiveness of using HCl instead of HF to remove oxide and metal contamination revealed that repetitive treatments with high-concentration HCl is a good protocol for Ge cleaning [34]. Meanwhile, a broader comparison between different acids including HF, HCl, HBr, and HI as cleaning agents proposed HBr and HI as the best cleaning agents for Ge [34]. However, a similar study also concluded that HCl is more effective to remove oxides and improve surface smoothness for Ge [34].

Simultaneously, researchers also explored the use of a mixture of H_2O_2:base (KOH, NH_3) as an etching agent for Germanium. This approach directly derives from the SC protocol for Silicon using H_2O:H_2O_2:NH_3 [25], where the H_2O_2 acts as an oxidizing agent [34]. Other groups also explored the use of H_2O_2 as an oxidizing agent, but using an acid (HCl) instead of a base for the solution [34]. They studied the dissolution kinetics of Germanium, comparing the results of electroless wet etching using HCl:H_2O_2 to electrochemical etching using HCl. However, the electroless results show an important non-uniformities in the roughness depending on the HCl concentration, and demonstrate that HCl electrochemical etching leads to the formation of tall pyramids of about 4 µm in height [34], a major problem when shallow pn junction devices are needed.

In this work, we report a new electroless chemical etching treatment to achieve uniform and shallow Ge nanopatterning yielding reduced optical reflectance for optoelectronic applications. This protocol relies on a specific mixture of HCl:HNO_3 at 3:1 concentrations or so-called aqua regia. Our analysis relies on SEM and AFM analysis to study the film morphology and surface characteristics. In addition, we use XRD, FTIR, and XPS to assess crystallinity and confirm a hydrogen passivation of the treated surface, which protects from native oxidation when exposed to air. Finally, reflectance measurements confirm that this electroless all solution-based protocol can significantly reduce reflectance using shallow nano-texturing of Germanium for device integration.

2. Results and Discussion

2.1. Structural Characterization by SEM

While Figure 1a represents a typical Germanium sample (as received), Figure 1b shows the surface after cleaning in a 37% HCl bath for 15 min at room temperature to remove the impurities observed on the cleaved wafers. Then, immersion in a 70% HNO_3 bath leads to a pronounced surface oxidation. Indeed, the SEM image shown in Figure 1c is a 45°-tilted top view of the edge of a clean Ge sample after 60 min oxidation in 70% HNO_3. Finally, the sample shown in Figure 1c was cleaved again using a diamond scriber to reveal a pristine edge used as a baseline to identify the species formed during HNO_3 bath immersion. Figure 1d shows the cleaved cross-section, identifying the two distinct regions analyzed under EDX with their respective elemental compositions shown in Table 1. Section 1 is the fresh untreated Ge and Section 2 is the oxidized GeO_x layer formed during HNO_3 bath immersion.
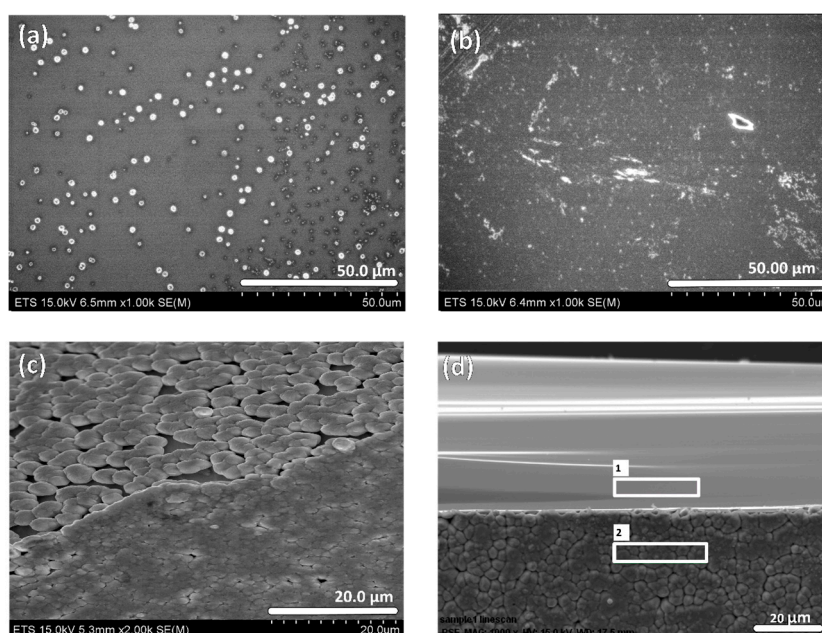
Figure 1. (**a**) Pristine n-type and Sb-doped Ge (100) surface without cleaning; (**b**) Sample after a 15-min immersion in concentrated 37% HCl bath; (**c**) Tilted (45°) view of a Ge sample's edge observed after a 60-min immersion in 70% HNO_3 bath; (**d**) Cross-sectional view of a Ge sample cleaved after a 60-min immersion in 70% HNO_3 bath. Section 1 and Section 2 were analyzed by EDX and their compositions are summarized in Table 1.

Table 1. Elemental analysis of the pristine untreated Germanium (Ge) (Section 1) and after a 60-min immersion in 70% HNO_3 bath (Section 2), as seen in Figure 1d.

Mass Percent (%)			
Sections	C	O	Ge
Section 1	1.95	–	98.05
Section 2	–	22.90	77.10

When using a mixture of HCl:HNO_3, we are expecting that HNO_3 will act as an oxidizing agent for Ge and will also bump HCl molecules off till their separation to let them further dissolve the Germanium. Hence, HCl (a halide like HF, HBr, and HI) will help to weaken interatomic bonds, allowing etching. As such, the experimental plan for such a mixture involves three key parameters: (1) HCl concentration; (2) HNO_3 concentration; and (3) bath temperature and immersion time. Here, we settled for a 3:1 solution of HCl:HNO_3 (aqua regia), and all immersions were performed at room temperature. We choose this particular aqua regia volumetric mixture 3:1 of concentrated HCl and HNO_3 because this makes the solution stronger which will attack more aggressively the Germanium substrate. 4:1 or 5:1 has less HNO_3 available so it is less aggressive.

Figure 2 shows typical SEM micrographs after immersion in the 3:1 aqua regia bath for 15 min at room temperature. The low-resolution micrograph in Figure 2a confirms the surface is uniformly etched, while the higher-resolution micrographs in Figure 2b,c clearly show the inverted-pyramid pit structures, indicating the anisotropy of the chemical etching process. This formation could be explained by the etching that happens along the low-energy planes of the diamond crystalline structure of the Ge.
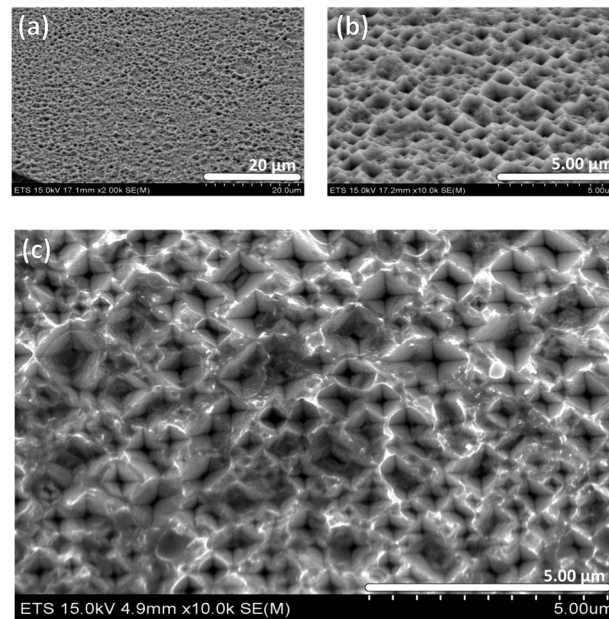
Figure 2. Etched Germanium sample after 15-min treatment in 3:1 Aqua Regia. (**a**) Tilted (45°) view at low resolution; (**b**) Tilted (45°) view at higher resolution; (**c**) Top-view of the inverted-pyramid pit structure at high resolution.

Lower magnification images illustrated in Figure 3 show the formation of long-range second-order circle-like features in the etching pattern, which are more clearly observed for very short (7-min) immersion times. These features stem from a H_2-bubbling phenomenon [35], which was later confirmed by chemical analysis of the surface. Stirring or depositing the beaker in the top of a vortex shaker in order to release the surface from the bubbles doesn't show any improvement: Neither by bare eyes nor under SEM microscope. However, a possible solution to alleviate this H_2-bubbling effect from the surface patterning will be to add a wetting agent to the solution.

To validate this hypothesis, we added ethanol in the same proportion as HNO_3 as a wetting agent in the solution. While the long-range circle-like features are certainly much less pronounced in Figure 3b, we find that some remnants of residual H_2-bubbling can still be seen on the wafer surface as shown in Figure 3c. Also, the reaction is not stable after about 7 min due to the probable formation of ethyl nitrate, $CH_3CH_2ONO_2$ [36]. So this enhancement is possible only for very short immersion times. However, this is not an issue here, as these features blend-in as the surface corrugations increases for longer etching times and the H_2 bubbles, when formed, are immediately released due to the surface passivation that will be discussed below.
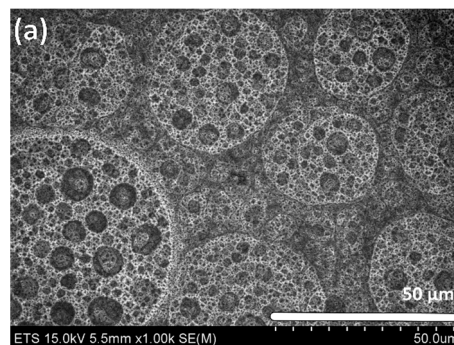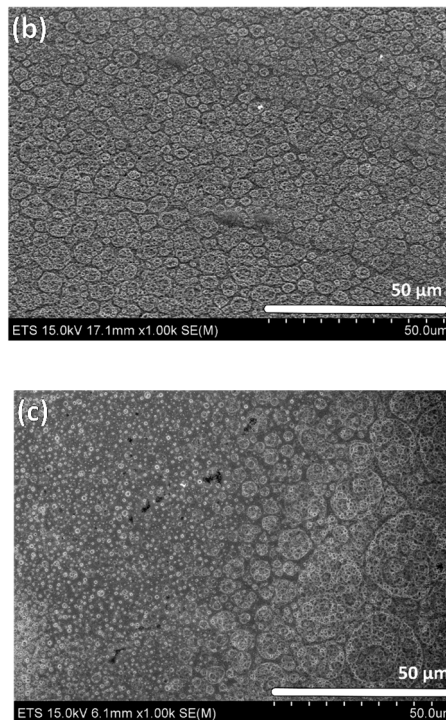

Figure 3. *Cont.*

Figure 3. Effect of the wetting agent (ethanol) on the H_2-bubbling consequences. (**a**) Top-view of a Ge sample following a 7-min immersion in aqua regia; (**b**) Tilted (45°) view of a Ge sample following a 7-min immersion in a mix of aqua regia with ethanol; (**c**) Top-view of (b).

2.2. Surface Morphology Studied by AFM

More careful AFM analysis shown in Figure 4 indicates how the surface morphology evolves by increasing the immersion time from 5 to 60 min. Except for some residual H_2 bubbling marks discussed in the previous section, the porous pit structures have distributed uniformly on the surface. Table 2 compares the surface statistics including roughness (R_a), mean and maximum heights (relative on the lowest point taken as reference) for increasing immersion times.

Table 2. Surface statistics for different immersion times ranging between 5 and 60 min based on the AFM images from Figure 4 analyzed using the Gwyddion freeware.

Sample	Immersion Time (min)	Mean Height (μm)	Maximum Height (μm)	Roughness (μm)
(a)	5	0.31	0.70	0.06
(b)	7	0.33	0.76	0.06
(c)	10	0.35	0.81	0.07
(d)	12	0.42	1.02	0.07
(e)	15	0.75	1.37	0.13
(f)	30	1.27	2.16	0.19
(g)	60	1.98	3.28	0.40

Figure 4. AFM images of Ge samples immersed in Aqua regia for (**a**) 5 min; (**b**) 7 min; (**c**) 10 min; (**d**) 12 min; (**e**) 15 min; (**f**) 30 min; and (**g**) 60 min.

Clearly, longer immersion times lead to a deeper etching. However, H_2 bubbling that stays attached to the surface eventually causes the etching to slow down in some regions and some stirring inside the solution. In Figure 5, we can observe a significant slowdown of the etching rate for longer immersion. We have explained this phenomenon in the next sections, when delving in to the surface chemistry analysis.
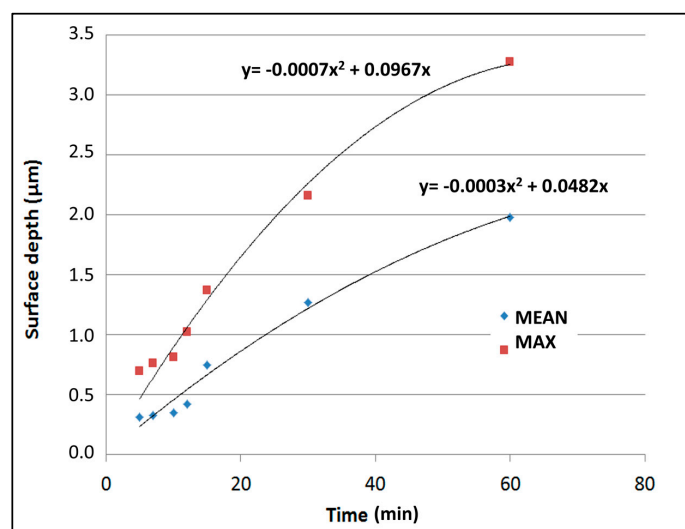

Figure 5. Evolution of the nanostructured surface depth with increasing immersion time in the aqua regia bath.

2.3. Structural Analysis Using X-ray Diffraction

Surface analysis using X-ray diffraction (XRD) has performed to determine the crystallinity of the etched sample and the crystallite size. The XRD data from Figure 6 reveals peaks corresponding to three different Ge lattice planes [37,38].
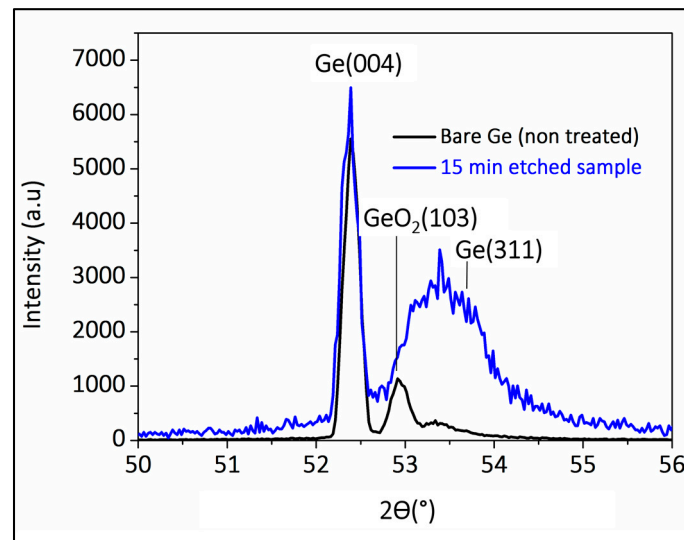

Figure 6. X-ray diffraction (XRD) of the cleaned Germanium before and after a 15-min immersion in the aqua regia solution.

The main peak corresponds to the (004) crystallographic orientation, followed by a second less intense peak closer to 53° and corresponding to the (103) crystallographic orientation for the bare Germanium. After etching, a broader peak centered at 53.5° corresponding to the (311) crystallographic orientation appears in the XRD data.

If we compare XRD results before and after the 15-min immersion in aqua regia, it suggests that the treatment has eliminated GeO_2 in the (103) plane [39], while promoting an etching along the (311) [40–42] direction (exposing this crystalline plane), to form the inverted pyramid structures.

Based on these data, the Scherer formula can evaluate the crystallites' average diameter L in the direction perpendicular to the plane hkl, under the assumption that the line broadening is mainly due to the fragmentation of the crystal in small areas of coherent diffraction size L (<1000 Å) occurring during the chemical etching. This parameter L will be estimated using the following equation [43]:

$$L \, hkl = \frac{0.9\lambda}{b \cos \theta} \tag{1}$$

where b is the angular full-width at half-maximum (FWHM) of the diffraction peaks, θ is the Bragg angle defined by the peak position and λ is the source wavelength ($K_{\alpha 1,2}$ of Copper = 1.5418 Å). The XRD data in Figure 6 allow calculation of the (311)-peak full-width at half-maximum (FWHM) for the etched samples of $1.0° \pm 0.1°$.

This calculation suggests that the crystallite size of the treated sample is 29.87 Å in the Ge (311) plane. In reality, this evolution is due to the growth of crystallites and can also be influenced slightly by experimental parameters such as local deformations induced by dislocations or variation of concentration in the case of solid solution [44].

Based on this analysis, the exposed facets in the inverse pyramid-shaped pits clearly seem to correspond to the (311) directions [45], and the diffraction peak evolution likely originates from concentration variations of the solid solution after etching in the perpendicular direction to the (311) plane [44].

2.4. Surface Chemistry Analysis Using FTIR Analysis

For potential device integration, it is essential to know the surface chemistry for the nano-textured Ge. In this section, we investigate how the aqua regia treatment affects the chemical nature and the chemistry of the exposed surface. In the FTIR spectroscopy results of both etched and non-etched Germanium samples shown in Figure 7, the assignment of peaks was based on several literature sources and it is summarized in Table 3. Even though the same frequency vibration could be assigned to more than one atomic group, we notice the domination over four types of atomic bonds: (1) a large Ge–H$_x$ vibration between 1875 and 2250 cm^{-1}; (2) O–H bonds which essentially appear between 3350 and 3855 cm^{-1}; (3) Carbon based vibrations in several frequencies; and (4) N–H vibrations.
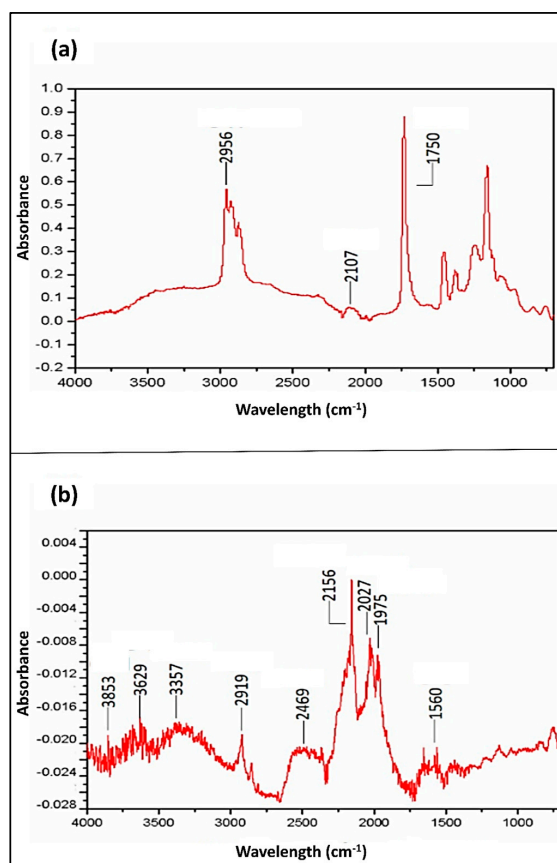

Figure 7. FTIR analysis of the Germanium sample. (**a**) Clean Germanium sample without any aqua regia treatment; (**b**) after a 15-min immersion in aqua regia at room-temperature.

Table 3. Attribution of infrared peaks to atomic bonds.

Valence Vibration Frequency (cm^{-1})	Attribution of Peaks to Atomic Bands	References
1560	N–H	[46]
1750	C=O	[46–48]
1975	Ge–H$_x$ (x = 1) or X=C=Y (X,Y)	[25,46,49–52]
2027	Ge–H$_x$ (x = 2) or X=C=Y	[25,46,49,51]
2107	C≡C	[46]
2156	Ge–H$_x$ (x = 3), X=C=Y or C≡C	[25,46,51]
2469	O–H	[46]
2919	C–H	[46,48]
2956	C–H	[46,48,49]
3357	N–H, O–H (H bonded) or O–H (carboxylic)	[46,48]
3629	Free O–H or C–H	[46,48]
3853	O–H (stretching absorption of COOH)	[53]

The most challenging ascription relates to the identification of the Ge–H$_x$ components of the etched sample. Based on the literature, the Ge–H vibration appears between 1950–1990 cm^{-1} [50], which is consistent with the peak found at 1975 cm^{-1}. Meanwhile, the 2027 cm^{-1} peak is most likely due to Ge–H$_2$ [51]. Due to the collision which may happen between the two H atoms during hydrogen desorption, the Ge–H$_2$ is unstable and can be easily reduced to monohydride [54].

Also, despite the fact that the 2156 cm^{-1} peak could be attributed to Ge–H$_3$ bonding vibration [55], this is still not favorable considering the reaction leads to the formation of H$_2$ in addition to H$_2$O. Indeed, the H$_2$ formation should dominate during the reaction enabling the etching of the surface. However, Ge–H$_3$ formation could be more favorable with more hydride in the reaction [51,56], if terminations activating GeH$_4$ are H$_3$, H$_2$ and H [51] or when working on removing H$_2$O$_2$-grown Germanium oxides (GeO$_x$, x = 1,2) using HF [56]. For all those reasons this peak is more likely to correspond to a C≡C bond and this suggestion will be supported later with XPS analysis.

As for the O–H peaks at 2469 cm^{-1} and between 3350 and 3855 cm^{-1}, they originate from hydrogen desorption, which expects to be accompanied by oxidation or hydroxylation of the surface [43]. Albeit the Ge–O$_2$ removal based on XRD analysis shown in Figure 6, the sub-oxide is more difficult to eliminate and the ≡GeOH can remain as a stable form of the surface species.

The carbon-binding vibrations suggest the existence of some C≡C, C–H, and C–O bonds. While some of the carbon could have an organic origin or could be due to the anterior characterizations, previous studies on the stabilization of Ge–H in the air have shown that it is often accompanied by hydrocarbon contamination of the surface [57].

Finally, for the etched sample, the two peaks at 1560 cm^{-1} and 3357 cm^{-1} could indicate the presence of an N–H bond. This is expected considering the fact of HNO$_3$ use.

Now, if we compare the two FTIR spectra of Figure 7, it is interesting to focus on the main vibrations related to the hydride termination (starting from 1900 cm^{-1}). In this region, bare Germanium reveals two peaks, at 2107 cm^{-1} and at 2956 cm^{-1}, both related to carbon vibrations.

Hence, it is clear that, except the C–H peak observed at 2919 cm^{-1} and 2956 cm^{-1} for the etched and the bare sample respectively, the hydride termination observed on the etched sample appears largely as a result of the treatment. However, the C≡C peak observed at 2107 cm^{-1} and at 2156 cm^{-1} for the etched and bare sample respectively, indicate, not a contamination due to an exposure to the air, but rather a polymerized carbon. This may due to previous SEM characterization. After a relatively long period under electron beam, the surface of germanium can become carbonized.

2.5. Deeper Understand of the Surface Chemistry Using XPS Analysis

XPS analysis was performed to better understand, identify, and quantify the elements at the surface and their bonding. Since we used HCl and HNO$_3$ to etch Germanium, Ge, O, H, Cl, and N compounds are expected. A lot of C is also expected as the surface exposed to air and it has undergone several characterizations before XPS analyzed. Two samples were analyzed: one pristine germanium (not etched) taken as a reference and one etched with Aqua regia for 15 min.

XPS analysis was first performed using both AlKα and MgKα sources as shown in Table 4, because some peaks are superposed. Indeed, the Auger electron peak of Ge is situated in the same binding energy range as chlorine when Mg is used, and thus not allowing to correctly identify the presence of chlorine. Similarly, the Auger electron peak is found in the oxygen binding energy range when Al is used, which does not allow a proper analysis of the oxygen peak. Since no chlorine was detected in two samples, high-resolution analysis were done only with MgKα radiation shown in Table 5.

Table 4. XPS overview analysis using MgKα and AlKα sources on pristine and 15 min etched Germanium.

| Element | Binding Energy (eV) | Relative Atomic % | | | |
| | | Measured with a MgKα Source | | Measured with a AlKα Source | |
		Pristine	15 min Etch	Pristine	15 min Etch
Ge	31.9	5.4	3.0	7.6	5.1
C	285.1	74.6	86.6	75.1	83.2
O	532.1	12.6	10.2	13.3	11.2
F	689.8	7.3	–	3.9	–
Zn	1021.7	–	0.2	–	0.4

Table 5. XPS high resolution analysis to identify qualitatively single or composed elements of the surface.

| Element | Binding Energy (eV) | Full Width Half Maximum (FWHM) | Identification | Relative Atomic % | |
				Pristine	15 min Etch
Ge	29.4	1.4	Ge^0	2.3	2.4
	30.2		Ge^{1+} (Ge–H or Ge$_x$O$_y$, $x = 2$, $y = 1$)	–	0.4
	32.2	2.0	Ge^{3+} (Ge$_x$O$_y$, $x = 2$, $y = 3$)	–	0.5
	33.0		Ge^{4+} (GeO$_2$)	3.3	–
C	285.0	1.3	C–C	80.7	81.8
	286.8	1.6	C–O	–	4.6
O	531.3		Ge–O, Ge–OH (hydroxyl in surface)	–	6.5
	532.0	2.2		13.7	–
	532.8		C–O	–	3.8

In the overview analysis, as shown in Table 4, we find an important fluorine contamination on the pristine Germanium and a low zinc contamination in the 15 min-etched sample. Those contaminations come from the improper handling of samples during the cleaning and previous characterizations, and they will not be the subject of interpretation. There is also a high carbon contamination on the surface of the two samples. As we explained previously, this may due to exposure to ambient air and previous SEM characterization. After a relatively long period under the electron beam inside SEM, the surface becomes carbonized and burned. This result is in agreement with FTIR spectroscopy in which we identified the existence of C≡C peaks in both etched and non-etched samples.

High-resolution analysis of the reference sample (pristine Ge) shows that the germanium present in the surface is in Ge^0 form (binding energy (BE) = 29.4 eV), non-oxidized, and in oxidized form GeO$_2$ (BE = 33.0 eV). The analysis of the carbon peak of this same sample shows a narrower peak (FWHM = 1.3 eV) than normal (normally FWHM = 1.6 eV) found when it comes to simple carbon contamination from hydrocarbons in the air. A narrower peak indicates a well-organized compound such as a polymer or high-density graphite. Finally, oxygen peak analysis indicates that the latter is present in part in Germanium oxide and hydroxyl groups in the surface.

Analysis of the 15-min etched sample shows that there is no more GeO$_2$ present on the surface of this sample and the most part of germanium is in the Ge^0 form. A small proportion of Ge^{1+} and Ge^{3+} are also found respectively at BE = 30.2 eV and at BE = 32.2 eV. The presence of a small quantity of Ge^{3+} shows the presence of a germanium sub-oxide Ge$_x$O$_y$ (y/x is about 3/2). The Ge^{1+} could similarly indicate a sub oxide Ge$_x$O$_y$ with y/x = 1/2, but it could also indicate Ge–H bonds [58]. An important carbon contamination is also present in this sample. As for the reference sample, this carbon contamination may come from polymerized carbon during SEM analysis previously made on these samples. This, thus confirms the attribution of the 2156 cm^{-1} peak in the FTIR analysis to C≡C and not to Ge–H$_3$. For the future, it would be required to do the surface analysis before SEM analysis.

In summary, the treatment using the mixture HCl:HNO$_3$ can lead to three possible scenarios regarding the surface chemistry: (1) The treated surface can be Cl terminated (Ge–Cl), (2) the treated

surface can be H terminated (Ge–H), and (3) the surface consists of free dangling bonds (no termination at all) and the samples, in this case, oxidize with air exposure.

As no chlorine (Cl) was detected, the Ge–Cl scenario can be readily dismissed. Moreover, the XRD and XPS results confirm that germanium dioxide (GeO$_2$) is efficiently cleaned and eliminated from the surface of the etched sample. This leaves only the hydrogen passivation (Ge–H) which the existence was discussed and supported by FTIR and XPS results shown in Tables 3 and 5.

Finally, the observation of oxygen peaks with BE = 531.3 eV and BE = 532 eV could equally indicate the probable presence of a small quantity of sub-oxide (Ge–O) or Ge–OH due to Hydroxyl desorption. This suggests either that Ge–O exists in the surface before the treatment and the surface was not fully hydrogenated after the treatment, either the adsorption of hydrogen in ambient air is accompanied with oxidation and hydroxylation, or both and this does not have adverse effect as the surface remains stable and does not oxidize during exposure to the air after treatment.

2.6. Broadband Reflectivity Measurements

Our main purpose consists in achieving controllable and uniform nano-texturing of Germanium at low costs is to reduce the intrinsically high reflectance of bulk Germanium to enhance the light coupling efficiency for future Ge-based optoelectronic devices such as photo-detectors and photovoltaic devices. Indeed, the inverted pyramid-structure will trap the incident light. This will be particularly useful for homo- or hetero- junction Ge-based optoelectronic devices since all the light is wanted to be absorbed at this level and photons should not transmit. To observe this improvement, we performed reflectance spectroscopy between 950–1700 nm as a function of the immersion time using a spectrophotometer equipped with a 60 mm integrating sphere. The choice of this specific wavelength regions is imposed by Ge bandgap which is equal to 0.67 eV at room temperature. As the band gap is inversely proportional to wavelength, this means that Ge is unable to absorb long wavelengths higher than $\lambda_{max} = \frac{hc}{E_g} = 1.85$ μm. Thus, this makes it suitable for near-infrared based opto-electronic devices such as photodiodes and solar cells just like Silicon for visible range (0.4–0.7 μm).

As shown in Figure 8, the pristine Germanium reflectance varies between 54.8–58.5% between 950 and 1700 nm. A quick 5-min etching already yields a 12–14% decrease in reflectance. A long immersion further decreases the reflectance, which falls under 15% for a 60-min immersion. Based on previous sections, this corresponds to a mean depth around 2 μm and can reach almost 4 μm in peak-to-peak height. For opto-electronic devices integration, the junction is generally located close to the surface which make etching times between 5 and 15 min the region of interest as it induces to the formation of porous structures with mean depths between 0.31 and 0.75 microns. Further etching is still possible with longer etching times as we can note for 30 and 60 min' baths.
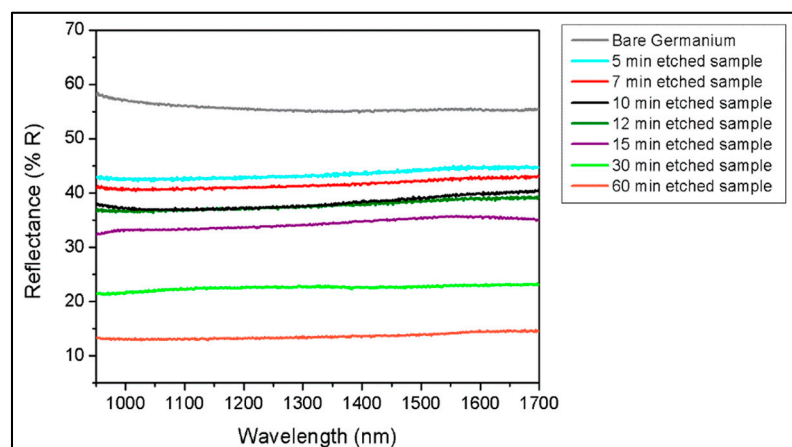

Figure 8. Broadband NIR reflectance of Germanium samples for increasing immersion times and comparison with a bare Ge sample.

As such, this low-cost aqua regia treatment can decrease the total reflectance and generate large gain in absorbance from 950 to 1700 nm. Figure 9 clearly shows that the decrease in reflectance slows down as the etching rate saturates for longer immersion, largely due to the Germanium surface passivation with hydrogen and the weakening of the etching power over time.
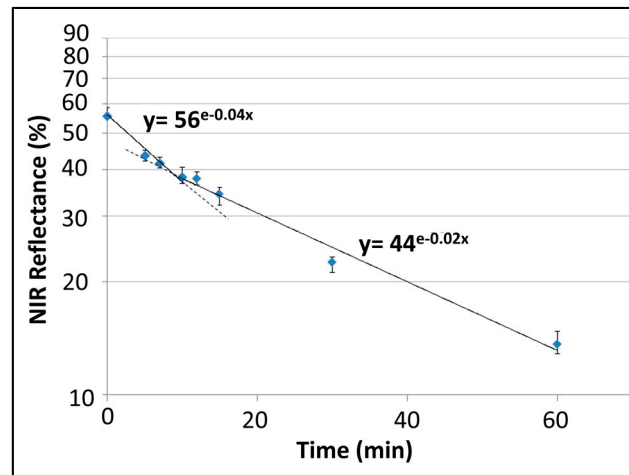

Figure 9. Average NIR reflectance (950–1700 nm) of Germanium samples for increasing immersion times and comparison with a pristine sample. The vertical bars show the minimum and maximum reflectance measured between 950 and 1700 nm for each etching time.

3. Materials and Methods

The nano-texturing process is entirely realized in a fume hood under ambient laboratory conditions. All samples are produced using commercial Sb-doped n-type Ge (100) wafers with resistivity ρ = 0.1–0.5 $\Omega \cdot$cm, which are purchased from MTI Corporation. These wafers are 2″ in diameter, 500 μm-thick and single-side polished (SSP). Nitric acid (HNO_3) at 70%, hydrochloric (HCl) acid at 37% and Hydrofluoric (HF) acid at 48% concentrations, purchased from Sigma-Aldrich (St. Louis, MI, USA), while deionized water (DI-H_2O) purchased from MAT laboratory.

First, the Ge wafers are cleaved into 1 cm^2 pieces using a diamond scriber, then dipped for 1 min in 2% HF, rinsed with DI-water and blow-dried with ultra-high purity nitrogen (N_2) gas. Then, cleaned samples are immersed immediately in a fresh aqua regia mixture (HCl:HNO_3 at 3:1). This 3:1 ratio refers to the respective volumes of HNO_3 and HCl solutions as received from Aldrich. After the desired etching time, the samples are removed from the solution bath and rinsed with DI-water, followed by N_2 blow-drying. The nanostructured Ge samples are then sealed in clean closed containers for the different characterizations.

The morphological characterization is performed using a field-emission scanning electron microscope (FE-SEM, model Hitachi SU-70, Schaumburg, IL, USA), while the topography of the resulting surface structure is measured using an atomic-force microscope (Bruker, Billerica, MA, USA, model Multimode 8 equipped with ScanAsyst scanning mode) and analyzed using the Gwyddion freeware to extract statistics pertaining to the pit structure and the surface roughness. Unfortunately, it wasn't possible to extract from the software the different values that the variable (height) can take from each iteration from pixel 1 to pixel n. So, it becomes not possible to calculate the standard variation around the mean height. However, it is important to precise that the mean height is calculated from the points defined by the pixels of the picture. For our measurements, we considered a picture of 512 by 512 pixels which results on n = 262.144 points. The mean height of 262.144 points is consequently very representative of the surface state.

For potential optoelectronic device integration, it is essential to acquire a clear understanding of the surface properties following the nano-patterning process. To do so, crystallinity is analysed

using theta-two-theta scan under X-ray diffraction (PANalytical X'Pert MRD 4-circle diffractometer, Amsterdam, The Netherlands), while atomic bonding on the surface is probed using FTIR (Thermo Scientific, Waltham, MA, USA, model Nicolet 6700 equipped with a Diamond Smart iTR Attenuated Total Reflectance module) and X-ray photoelectron spectroscopy (VG instrument, Waltham, MA, USA, model ESCALAB 3-MKII) equipped with an MgK_α and an AlK_α beam sources.

Finally, the surface reflectance is measured using an NIR spectrophotometer (Perkin Elmer, Waltham, MA, USA, model Lambda 750) equipped with a 60 mm integrating sphere. The UV-VIS-NIR spectrophotometer setup consists of several blocks and compartments. First, we find the source system with its two deuterium and halogen lamp. Depending on UV, VIS, or NIR region, the appropriate source is selected. Then, the light passes through a monochromator which selects the wavelength depending on the selected range and the interval between two consecutive data. Once the monochromatic light is selected, this one should be free of noise. For this reason, the flux passes through a filter system to eliminate every kind of noise and to make the light smooth. At this level, the light will be directed to the chopper and will split to two identical quantities: One will be directed to incite a reference sample and the other one will be directed to incite the sample we want to characterize. Now, it is important to zoom-in the samples compartment. The samples are positioned at a tilt angle of 8° from the vertical. It is of course important to mention that the light coming from the source and directed toward the samples is oriented through different optical lenses and that the flux goes through a 60-mm integrating sphere before hitting the concerned surface. Samples are positioned on two different walls of this integrated sphere. Thereby, the reflected rays undergo different reflection inside the sphere in order to make uniform information, which will be read from the detector placed in the top of the integrated sphere. The detection system is constituted of a multiplier PMT for UV-VIS range and of a lead sulfide cell PBS for NIR range, which is the range of our interest. The use of an integrating sphere and a reference sample allow us to measure accurate relative percentages of reflectance.

4. Conclusions

Our results clearly show that the surface treatment using 3:1 aqua regia ($HCl:HNO_3$) can allow a controllable, relatively uniform, and shallow nano-texturing of Germanium. Care should be taken to minimize the H_2-bubbling, which can lead to a long-range second-order patterning of the surface for very short immersion times (under 15 min). Our results show that the anisotropic etching preserves the crystallinity while the etching occurs in a preferential direction along the Ge (311) planes, yielding inverted pyramid-shaped pit structures. Meanwhile, our results also suggest that the exposed Ge surface is hydrogen-passivated (Ge–H). This is particularly interesting as previous reports suggested that treatments using only HCl lead to Ge–Cl rather than Ge–H termination because of its higher bond energy [59,60]. Our experiments suggest that the addition of HNO_3 in the mixture leads to the opposite result.

In summary, the aqua regia protocol provides a clean and dioxide-free nano-textured surface, which is also surface-stable and resistant to native oxidation due to hydrogen-passivation. The surface parameters' evolution as a function of the immersion time shows that the process can relatively be well controlled to achieve the desired characteristics. Depending on the immersion (etching) time, the NIR reflectance can be reduced under 15% using a 2 μm-deep nanopatterning.

In the future, we believe this facile all solution-based surface treatment could be most useful to achieve low-reflectance across a broad spectrum to improve Ge-based optoelectronic devices.

Author Contributions: Ibtihel Chaabane has established the synthesis and the material's characterization method of the nano-textured Germanium surface. Debika Banerjee has participated in the chemical laboratory experiments and the presentation of FTIR and UV-VIS graphs. The interpretations of the results and the data analyzes were discussed between Ibtihel Chaabane, Debika Banerjee, Oualid Touayar and Sylvain G. Cloutier The first draft of this manuscript was written by Ibtihel Chaabane, corrected by Sylvain G. Cloutier and Oualid Touayar.

Ibtihel Chaabane and Debika Banerjee have worked on the form editing of the manuscript and all authors have revised the manuscript before the final version and approved the content before submission.

Conflicts of Interest: The authors declare no conflict of interest.

References

1. Reinhardt, K.A.; Reidy, R.F. *Handbook for Cleaning for Semiconductor Manufacturing: Fundamentals and Applications*; John Wiley & Sons: Hoboken, NJ, USA, 2011; Volume 67.
2. Loscutoff, P.W.; Bent, S.F. Reactivity of the germanium surface: Chemical passivation and functionalization. *Ann. Rev. Phys. Chem.* **2006**, *57*, 467–495. [CrossRef] [PubMed]
3. Ramana, C.; Carbajal-Franco, G.; Vemuri, R.; Troitskaia, I.; Gromilov, S.; Atuchin, V. Optical properties and thermal stability of germanium oxide (GeO_2) nanocrystals with *α*-quartz structure. *Mater. Sci. Eng. B* **2010**, *174*, 279–284. [CrossRef]
4. Terakado, N.; Tanaka, K. Photo-induced phenomena in sputtered GeO_2 films. *J. J. Non-Cryst. Solids* **2005**, *351*, 54–60. [CrossRef]
5. Jiang, Z.; Xie, T.; Wang, G.; Yuan, X.; Ye, C.; Cai, W.; Meng, G.; Li, G.; Zhang, L. GeO_2 nanotubes and nanorods synthesized by vapor phase reactions. *Mater. Lett.* **2005**, *59*, 416–419. [CrossRef]
6. Su, Y.; Liang, X.; Li, S.; Chen, Y.; Zhou, Q.; Yin, S.; Meng, X.; Kong, M. Self-catalytic VLS growth and optical properties of single-crystalline GeO_2 nanowire arrays. *Mater. Lett.* **2008**, *62*, 1010–1013. [CrossRef]
7. Chen, X.; Cai, Q.; Zhang, J.; Chen, Z.; Wang, W.; Wu, Z.; Wu, Z. Synthesis and growth of germanium oxide nanoparticles in AOT reversed micelle. *Mater. Lett.* **2007**, *61*, 535–537. [CrossRef]
8. Kim, H.W.; Shim, S.H.; Lee, J.W. Cone-shaped structures of GeO_2 fabricated by a thermal evaporation process. *Appl. Surf. Sci.* **2007**, *253*, 7207–7210. [CrossRef]
9. Poerschke, R.; Madelung, O. *Data in Science and Technology, Semiconductors Group IV Elements and III–V Compounds*; Springer: Berlin, Germany, 1991.
10. Tsakalakos, L.; Balch, J.; Fronheiser, J.; Korevaar, B.; Sulima, O.; Rand, J. Silicon nanowire solar cells. *Appl. Phys. Lett.* **2007**, *91*, 233117. [CrossRef]
11. Hu, L.; Chen, G. Analysis of optical absorption in silicon nanowire arrays for photovoltaic applications. *Nano Lett.* **2007**, *7*, 3249–3252. [CrossRef] [PubMed]
12. Peng, K.Q.; Lee, S.T. Silicon nanowires for photovoltaic solar energy conversion. *Adv. Mater.* **2011**, *23*, 198–215. [CrossRef] [PubMed]
13. Tsakalakos, L.; Balch, J.; Fronheiser, J.; Shih, M.-Y.; LeBoeuf, S.F.; Pietrzykowski, M.; Codella, P.J.; Korevaar, B.A.; Sulima, O.V.; Rand, J. Strong broadband optical absorption in silicon nanowire films. *J. Nanophotonics* **2007**, *1*, 013552. [CrossRef]
14. Garnett, E.; Yang, P. Light trapping in silicon nanowire solar cells. *Nano Lett.* **2010**, *10*, 1082–1087. [CrossRef] [PubMed]
15. Li, X. Metal assisted chemical etching for high aspect ratio nanostructures: A review of characteristics and applications in photovoltaics. *Curr. Opin. Solid State Mater. Sci.* **2012**, *16*, 71–81. [CrossRef]
16. Qu, Y.; Liao, L.; Li, Y.; Zhang, H.; Huang, Y.; Duan, X. Electrically conductive and optically active porous silicon nanowires. *Nano Lett.* **2009**, *9*, 4539–4543. [CrossRef] [PubMed]
17. Hung, Y.-J.; Lee, S.-L.; Wu, K.-C.; Tai, Y.; Pan, Y.-T. Antireflective silicon surface with vertical-aligned silicon nanowires realized by simple wet chemical etching processes. *Opt. Express* **2011**, *19*, 15792–15802. [CrossRef] [PubMed]
18. Geyer, N.; Fuhrmann, B.; Huang, Z.; de Boor, J.; Leipner, H.S.; Werner, P. Model for the mass transport during metal-assisted chemical etching with contiguous metal films as catalysts. *J. Phys. Chem. C* **2012**, *116*, 13446–13451. [CrossRef]
19. Peng, K.; Fang, H.; Hu, J.; Wu, Y.; Zhu, J.; Yan, Y.; Lee, S. Metal-Particle-Induced, Highly Localized Site-Specific Etching of Si and Formation of Single-Crystalline Si Nanowires in Aqueous Fluoride Solution. *Chem. A Eur. J.* **2006**, *12*, 7942–7947. [CrossRef] [PubMed]
20. Fang, C.; Föll, H.; Carstensen, J. Electrochemical pore etching in germanium. *J. Electroanal. Chem.* **2006**, *589*, 259–288. [CrossRef]
21. Garralaga Rojas, E.; Hensen, J.; Carstensen, J.; Föll, H.; Brendel, R. Porous germanium multilayers. *Phys. Status Solidi C* **2011**, *8*, 1731–1733. [CrossRef]

22. Akkari, E.; Benachour, Z.; Aouida, S.; Touayar, O.; Bessais, B.; Benbrahim, J. Study and characterization of porous germanium for radiometric measurements. *Phys. Status Solidi C* **2009**, *6*, 1685–1688. [CrossRef]

23. Rojas, E.G.; Terheiden, B.; Plagwitz, H.; Hensen, J.; Baur, C.; Strobl, G.F.; Brendel, R. Formation of mesoporous germanium double layers by electrochemical etching for layer transfer processes. *Electrochem. Commun.* **2010**, *12*, 231–233. [CrossRef]

24. Rojas, E.G.; Hensen, J.; Baur, C.; Brendel, R. Sintering and reorganization of electrochemically etched mesoporous germanium layers in various atmospheres. *Sol. Energy Mater. Sol. Cells* **2011**, *95*, 292–295. [CrossRef]

25. Marsella, J.; Durham, D.; Molnar, L. *Handbook of Cleaning for Semiconductor Manufacturing*; Scrivener Publishing LLC: Beverly, MA, USA, 2011.

26. Adhikari, H.; Sun, S.; Pianetta, P.; Chidsey, C.E.; McIntyre, P.C. *Surface Passivation of Germanium Nanowires*; Stanford Linear Accelerator Center: Menlo Park, CA, USA, 2005.

27. Bodlaki, D.; Yamamoto, H.; Waldeck, D.; Borguet, E. Ambient stability of chemically passivated germanium interfaces. *Surf. Sci.* **2003**, *543*, 63–74. [CrossRef]

28. Souriau, L.; Terzieva, V.; Meuris, M.; Caymax, M. A Wet Etching Technique to Reveal Threading Dislocations in Thin Germanium Layers. *Solid State Phenom.* **2008**, *134*, 83–86. [CrossRef]

29. Leancu, R.; Moldovan, N.; Csepregi, L.; Lang, W. Anisotropic etching of germanium. *Sens. Actuators A Phys.* **1995**, *46*, 35–37. [CrossRef]

30. Jing, C.; Zhang, C.; Zang, X.; Zhou, W.; Bai, W.; Lin, T.; Chu, J. Fabrication and characteristics of porous germanium films. *Sci. Technol. Adv. Mater.* **2009**, *10*, 065001. [CrossRef] [PubMed]

31. Sun, S.; Sun, Y.; Liu, Z.; Lee, D.-I.; Peterson, S.; Pianetta, P. Surface termination and roughness of Ge (100) cleaned by HF and HCl solutions. *Appl. Phys. Lett.* **2006**, *88*, 021903. [CrossRef]

32. Schwartz, B.; Robbins, H. Chemical etching of germanium in solutions of HF, HNO$_3$, H$_2$O, and HC$_2$H$_3$O$_2$. *J. Electrochem. Soc.* **1964**, *111*, 196–201. [CrossRef]

33. Kern, W. Cleaning solutions based on hydrogen peroxide for use in silicon semiconductor technology. *RCA Rev.* **1970**, *31*, 187–206.

34. Sioncke, S.; Brunco, D.P.; Meuris, M.; Uwamahoro, O.; Van Steenbergen, J.; Vrancken, E.; Heyns, M.M. Etch Rates of Ge, GaAs and InGaAs in Acids, Bases and Peroxide Based Mixtures. *ECS Trans.* **2008**, *16*, 451–460.

35. Garralaga Rojas, E.J. Mesoporous Germanium Layer Formation by Electrochemical Etching. Ph.D. Thesis, Christian-Albrechts Universität Kiel, Kiel, Germany, 2010.

36. Murray, P.R. *Principles of Organic Chemistry: A Modern and Comprehensive Text for Schools and Colleges*; Heinemann: Oxford, UK, 1977.

37. Ballato, J.; Hawkins, T.; Foy, P.; Yazgan-Kokuoz, B.; Stolen, R.; McMillen, C.; Hon, N.; Jalali, B.; Rice, R. Glass-clad single-crystal germanium optical fiber. *Opt. Express* **2009**, *17*, 8029–8035. [CrossRef] [PubMed]

38. Ko, C.-Y.; Lin, W.-T. SiO$_2$-and CuO-enhanced growth of Ge–Si1−*x*Ge*x*O*y* and GeO$_2$–Si1−*x*Ge*x*O*y* core–shell nanowires on a Si substrate via carbothermal reduction. *Nanotechnology* **2006**, *17*, 4464. [CrossRef]

39. Jia, H.; Kloepsch, R.; He, X.; Badillo, J.P.; Winter, M.; Placke, T. One-step synthesis of novel mesoporous three-dimensional GeO 2 and its lithium storage properties. *J. Mater. Chem. A* **2014**, *2*, 17545–17550. [CrossRef]

40. Chopra, K.; Major, S.; Pandya, D. Transparent conductors—A status review. *Thin Solid Films* **1983**, *102*, 1–46. [CrossRef]

41. Robinson, J.T. *Germanium Island Assembly on Metal-Patterned Silicon*; ProQuest: Berkeley, CA, USA, 2007.

42. Wedler, G. Introduction to the Properties of Crystal Surfaces. *Z. Phys. Chem.* **1975**, *96*, 175. [CrossRef]

43. Patterson, A. The Scherrer formula for X-ray particle size determination. *Phys. Rev.* **1939**, *56*, 978. [CrossRef]

44. Degallaix, S. *Caractérisation Expérimentale des Matériaux*; Presses Polytechniques et Universitaires Romandes: Lausanne, Switzerland, 2007.

45. Stekolnikov, A.; Bechstedt, F. Shape of free and constrained group-IV crystallites: Influence of surface energies. *Phys. Rev. B* **2005**, *72*, 125326. [CrossRef]

46. Pavia, L.D.; Lampman, G.M.; Kriz, G.S.; Vyvyan, J.R. *Introduction to Spectroscopy*, 5th ed.; CENGAGE Learning: Boston, MA, USA, 2013.

47. Das, S.K.; Mahanta, S.P.; Bania, K.K. Oxidative coupling of 2-naphthol by zeolite-Y supported homo and heterometallic trinuclear acetate clusters. *RSC Adv.* **2014**, *4*, 51496–51509. [CrossRef]

48. Kunst, S.R.; Beltrami, L.V.R.; Cardoso, H.R.P.; Santana, J.A.; Sarmento, V.H.V.; Müller, I.L.; Malfatti, C.D.F. Characterization of Siloxane-poly (methyl methacrylate) Hybrid Films Obtained on a Tinplate Substrate Modified by the Addition of Organic and Inorganic Acids. *Mater. Res.* **2015**, *18*, 151–163. [CrossRef]

49. Choi, H.C.; Buriak, J.M. Preparation and functionalization of hydride terminated porous germanium Electronic supplementary information (ESI) available: FTIR thermal stability measurements and SEM images. *Chem. Commun.* **2000**, 1669–1670. [CrossRef]

50. Maroun, F.; Ozanam, F.; Chazalviel, J.-N. In-situ infrared monitoring of surface chemistry and free-carrier concentration correlated with voltammetry: Germanium, a model electrode. *J. Phys. Chem. B* **1999**, *103*, 5280–5288. Available online: http://www.rsc.org/suppdata/cc/b0/b004011h (accessed on 15 November 2015). [CrossRef]

51. Arrais, A.; Benzi, P.; Bottizzo, E.; Demaria, C. Correlations among hydrogen bonding configuration, structural order and optical coefficients in hydrogenated amorphous germanium obtained by X-ray-activated chemical vapour deposition. *J. Phys. D Appl. Phys.* **2009**, *42*, 105406. [CrossRef]

52. Abo-Ghazala, M.; Hazrny, S.A. Hydrogen bonding in hydrogenated amorphous germanium. *Tsinghua Sci. Technol.* **2004**, *9*, 177–180.

53. Sunatkari, A.; Talwatkar, S.; Tamgadge, Y.; Muley, G. Synthesis, Characterization and Optical Properties of L-Arginine Stabilized Gold Nanocolloids. *Nanosci. Nanotechnol.* **2015**, *5*, 30–35.

54. Maeng, J.Y.; Lee, J.Y.; Cho, Y.E.; Kim, S.; Jo, S.K. Surface dihydrides on Ge (100): A scanning tunneling microscopy study. *J. Abbr.* **2002**, *81*, 3555. [CrossRef]

55. Tice, J.B. Synthesis and Fundamental Studies of Novel Main Group IV and Azidoarsenic CVD Precursors. Ph.D. Thesis, Arizona State University, Tempe, AZ, USA, 2008.

56. Rivillon, S.; Chabal, Y.J.; Amy, F.; Kahn, A. Hydrogen passivation of germanium (100) surface using wet chemical preparation. *Appl. Phys. Lett.* **2005**, *87*, 253101. [CrossRef]

57. Amy, S.R.; Chabal, Y.J.; Amy, F.; Kahn, A.; Krugg, C.; Kirsch, P. Wet Chemical Cleaning of Germanium Surfaces for Growth of High-k Dielectrics. Proceedings of MRS Proceedings, San Francisco, CA, USA, 1 December 2006; Volume 917. [CrossRef]

58. Adhikari, H.; McIntyre, P.C.; Sun, S.; Pianetta, P.; Chidsey, C.E. Photoemission studies of passivation of germanium nanowires. *Appl. Phys. Lett.* **2005**, *87*, 263109. [CrossRef]

59. Lu, Z. Air-stable Cl-terminated Ge (111). *Appl. Phys. Lett.* **1996**, *68*, 520–522. [CrossRef]

60. Lu, Z.; Tyliszczak, T.; Hitchcock, A.; Dharma-Wardana, M. Structure of the Cl-passivated Ge (111) surface determined using X-ray absorption and first principles calculations. *Surf. Sci.* **1999**, *442*, L948–L952. [CrossRef]